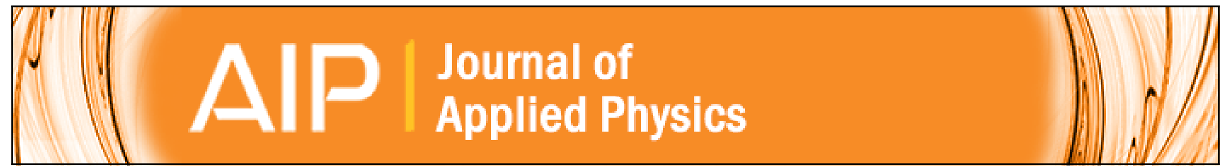

Modeling small-signal response of GaN-based metal-insulator-semiconductor high electron mobility transistor gate stack in spill-over regime: Effect of barrier resistance and interface states

M. Capriotti, P. Lagger, C. Fleury, M. Oposich, O. Bethge, C. Ostermaier, G. Strasser, and D. Pogany

Citation: Journal of Applied Physics **117**, 024506 (2015); doi: 10.1063/1.4905945
View online: http://dx.doi.org/10.1063/1.4905945
View Table of Contents: http://scitation.aip.org/content/aip/journal/jap/117/2?ver=pdfcov
Published by the AIP Publishing

Articles you may be interested in

Gate-control efficiency and interface state density evaluated from capacitance-frequency-temperature mapping for GaN-based metal-insulator-semiconductor devices
J. Appl. Phys. **116**, 184507 (2014); 10.1063/1.4901290

On the origin of the two-dimensional electron gas at AlGaN/GaN heterojunctions and its influence on recessed-gate metal-insulator-semiconductor high electron mobility transistors
J. Appl. Phys. **116**, 134506 (2014); 10.1063/1.4896900

Role of the dielectric for the charging dynamics of the dielectric/barrier interface in AlGaN/GaN based metal-insulator-semiconductor structures under forward gate bias stress
Appl. Phys. Lett. **105**, 033512 (2014); 10.1063/1.4891532

Atomic layer deposition of ZrO2 as gate dielectrics for AlGaN/GaN metal-insulator-semiconductor high electron mobility transistors on silicon
Appl. Phys. Lett. **103**, 142109 (2013); 10.1063/1.4824445

GaN metal–insulator–semiconductor high-electron-mobility transistor with plasma enhanced atomic layer deposited AlN as gate dielectric and passivation
J. Vac. Sci. Technol. B **31**, 052201 (2013); 10.1116/1.4816477

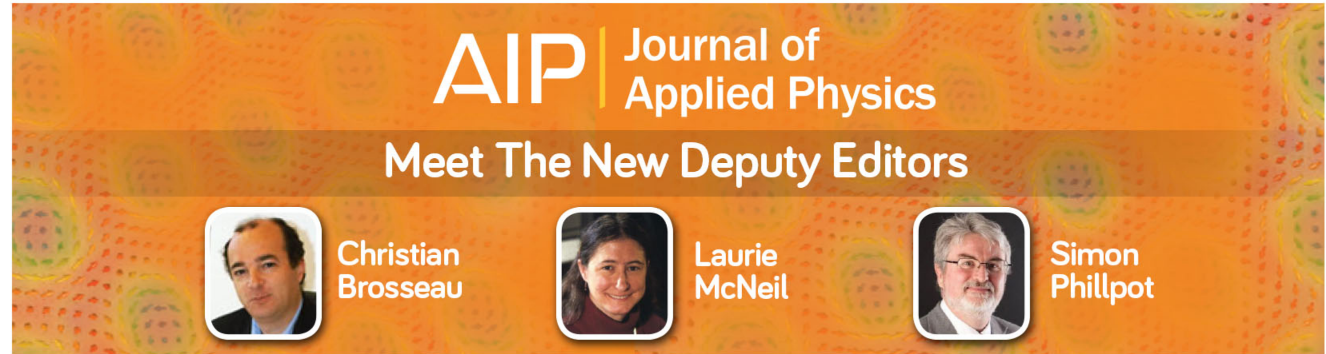

[This article is copyrighted as indicated in the article. Reuse of AIP content is subject to the terms at: http://scitation.aip.org/termsconditions. Downloaded to] IP: 128.131.87.29 On: Wed, 28 Jan 2015 15:02:39

JOURNAL OF APPLIED PHYSICS **117**, 024506 (2015)

Modeling small-signal response of GaN-based metal-insulator-semiconductor high electron mobility transistor gate stack in spill-over regime: Effect of barrier resistance and interface states

M. Capriotti,[1,a)] P. Lagger,[1,2] C. Fleury,[1] M. Oposich,[1] O. Bethge,[1] C. Ostermaier,[2] G. Strasser,[1] and D. Pogany[1,a)]
[1]*Institute for Solid State Electronics, Vienna University of Technology, Floragasse 7, A-1040 Vienna, Austria*
[2]*Infineon Technologies Austria AG, Siemensstraße 2, A-9500 Villach, Austria*

(Received 6 October 2014; accepted 3 January 2015; published online 13 January 2015)

We provide theoretical and simulation analysis of the small signal response of SiO_2/AlGaN/GaN metal insulator semiconductor (MIS) capacitors from depletion to spill over region, where the AlGaN/SiO_2 interface is accumulated with free electrons. A lumped element model of the gate stack, including the response of traps at the III-N/dielectric interface, is proposed and represented in terms of equivalent parallel capacitance, C_p, and conductance, G_p. C_p -voltage and G_p -voltage dependences are modelled taking into account bias dependent AlGaN barrier dynamic resistance R_{br} and the effective channel resistance. In particular, in the spill-over region, the drop of C_p with the frequency increase can be explained even without taking into account the response of interface traps, solely by considering the intrinsic response of the gate stack (i.e., no trap effects) and the decrease of R_{br} with the applied forward bias. Furthermore, we show the limitations of the conductance method for the evaluation of the density of interface traps, D_{it}, from the G_p/ω vs. angular frequency ω curves. A peak in G_p/ω *vs.* ω occurs even without traps, merely due to the intrinsic frequency response of gate stack. Moreover, the amplitude of the G_p/ω *vs.* ω peak saturates at high D_{it}, which can lead to underestimation of D_{it}. Understanding the complex interplay between the intrinsic gate stack response and the effect of interface traps is relevant for the development of normally on and normally off MIS high electron mobility transistors with stable threshold voltage. © *2015 AIP Publishing LLC*. [http://dx.doi.org/10.1063/1.4905945]

I. INTRODUCTION

GaN-based metal-insulator-semiconductor high-electron-mobility transistors (MIS-HEMTs) are attractive candidates for efficient power conversion due to low gate leakage current, large gate voltage swing, and high mobility of the two-dimensional electron gas (2DEG) channel.[1–6] Despite the advantages, MIS-HEMTs still suffer from threshold voltage (V_{th}) instability under forward biasing conditions.[7–9] The V_{th} instability is mainly attributed to trapping phenomena occurring at the III-N/dielectric interface.[7–9] This interface is known to be affected by interface states with high density D_{it}, where both donor-like and acceptor-like states may be involved.[7,10–13] Several methods have been applied to determine D_{it}. Capacitance techniques, measuring the capacitance-voltage (CV) hysteresis or the shape of the CV curve, are used for trap density determination.[3,4,7] Recently, stress-recovery experiments were used to study the dynamics of capture and emission from interface states and a broad distribution of time constants has been found.[8] It has also been pointed out that due to the latter effect, the small signal alternative current (*ac*) response and large signal slow drift phenomena are linked together in CV analysis.[9]

On the other hand, in the spill-over regime, where a second conductive channel is formed at the III-N/dielectric interface at forward gate bias, the onset of the second capacitance rise at the spillover voltage V_{so} is usually strongly frequency dependent.[7,14] It has recently been shown that the threshold voltage dynamics is governed not only by the capture and emission processes of traps at/near the dielectric/III-N interface but also by the effect of the conductance of the III-N barrier.[8] Yang *et al.* pointed out that the III-N barrier resistance could influence the extracted trap density using the conductance technique.[14] Therefore, they proposed to analyze the frequency and temperature dependence of V_{so} for the trap density evaluation.

In this paper, we enhance the lumped element model (LEM) analysis of Ref. 14 and provide an improved LEM for the admittance of the MIS-HEMT gate stack taking into account bias-dependent elements, with and without considering the response of traps. Using theoretical analysis and simulations, we show that, although the response of traps can indeed shift V_{so} with frequency, the same phenomenon can be alternatively explained by the intrinsic frequency response of the gate stack (i.e., without considering the response of traps) taking into account the voltage dependent III-N barrier dynamic resistance (R_{br}). We also analyze and discuss limitations of conductance method to evaluate the interface trap density in MIS-HEMTs. Our goal, using such LEM analysis, is to provide physical insight into complex interdependence between the intrinsic response of the gate stack and effects of traps, showing that they can contribute comparably to the total response. The paper is organized as

a)Authors to whom correspondence should be addressed. Electronic addresses: mattia.capriotti@tuwien.ac.at and dionyz.pogany@tuwien.ac.at

 © 2015 AIP Publishing LLC

[This article is copyrighted as indicated in the article. Reuse of AIP content is subject to the terms at: http://scitation.aip.org/termsconditions. Downloaded to] IP: 128.131.87.29 On: Wed, 28 Jan 2015 15:02:39

FIG. 1. (a) Schematics of the studied MIS-structure; (b) LEM for the spill-over region without traps; (c) equivalent parallel capacitance C_p and conductance G_p, (d) LEM for the entire bias regime; (e) LEM for the trap with single energy level and single time constant, (f) LEM for multiple defects, (g) LEM with traps where the defect branch is given in parallel representation. Legend: C_{ox} is the gate oxide/dielectrics, C_{br} is the barrier capacitance, R_{br} (G_{br}) is the barrier resistance (conductance), C_d is the depletion capacitance, R_c is channel resistance, C_s is the substrate capacitance, $C_{t,s}$ and $G_{t,s}$ are the serial representation of frequency independent trap capacitance and conductance, respectively, $G_{br,T}$ is the barrier conductance in series to the trap, $C_{t,p}$ and $G_{t,p}$ are equivalent parallel capacitance and conductance representations of the defect branch from (e), respectively.

follows: Sec. II presents device details and experiments. Section III A gives analytical expressions for the equivalent parallel capacitance C_p and conductance G_p and theoretical analysis in the spill-over regime. Section III B presents LEM and simulation of C_p-voltage (C_p-V) and G_p-voltage (C_p-V) curves from depletion to spill-over region without traps. Section III C presents the LEM with traps in the spill-over regime. The corresponding simulated C_p-V and G_p/ω *vs.* angular frequency ω dependences are given and discussed in Sections III D and III E, respectively, followed by Sec. IV.

II. DEVICE STRUCTURE AND EXPERIMENTS

The heterostructure material is composed of the following layers from top to down: 25 nm $Al_{0.25}Ga_{0.75}N$, 1 nm AlN spacer, 2 μm thick GaN channel/buffer layer, and AlGaN nucleation layer grown by metal organic chemical vapor deposition on highly doped silicon substrate, see Fig. 1(a). A 30 nm SiO_2 layer was chemical vapor deposited on top of the heterostructure, forming thus a MIS heterostructure capacitor, here shortly MIS structure. Capacitor top electrode is from Pt/Au (area of 2000 μm^2) and the back contact on Si was achieved by Al alloying. The chip size of 2 cm^2 assures that the Si substrate to 2DEG capacitance, C_s, which is of the order of 10 nF (see Fig. 1(a)), is much larger than the capacitance of the studied MIS capacitor, measuring thus the response of the latter (since the structure is normally on the 2DEG spreads over the whole chip). Circular Schottky diodes of the same area were also fabricated and characterized for the reference purpose. The CV analysis was performed with a Keithley 4200 using an equivalent parallel capacitance/conductance model (see Fig. 1(c)). Due to existing V_{th} instabilities and interlinking of *ac* response and slow drifts,[9,15] the voltage sweep was performed several times for each frequency for the same starting biasing conditions and same time between the measurements. Thus some typical behavior with quasi-stable hysteresis was repeatedly observed in CV curves for particular frequency. So the effect of slow recovery transients (i.e., initial threshold voltage shift) can be disregarded, allowing us to assume that the measured effect of frequency on CV curve dominates over the slow drifts due to trapping. Typical remaining maximum hysteresis between up and down sweeps for a sweeping rate of 10 V/min was about 0.3 V.

The measured CV and conductance-voltage (GV) curves from the depletion to the spill-over are given in Fig. 2; the frequency is given as parameter. With the frequency increase, the CV curves exhibit a shift in V_{so} to higher voltages. The capacitance values for the accumulation region (i.e., 2DEG in the GaN channel) and in the spillover region ($V > V_{so}$) approach the expected values of $C_{ox}C_{br}/(C_{ox} + C_{br})$ and C_{ox}, respectively. We also remark the existence of a conductance peak for all frequencies near V_{th} and for low frequency curves near V_{so}.

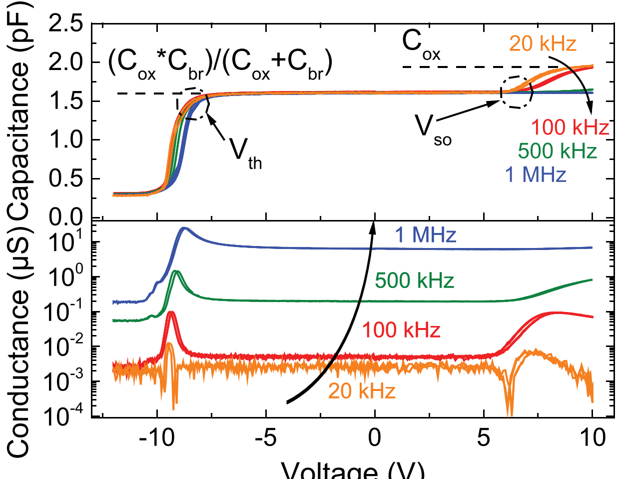

FIG. 2. Measured equivalent parallel capacitance C_p and conductance G_p as a function of voltage for different frequencies. The plotted curves represent a typical curve (up and down sweep) for a particular frequency. The conductance measurements at 20 kHz exhibiting large noise are at the limit of accuracy.

[This article is copyrighted as indicated in the article. Reuse of AIP content is subject to the terms at: http://scitation.aip.org/termsconditions. Downloaded to] IP: 128.131.87.29 On: Wed, 28 Jan 2015 15:02:39

In order to find the bias-dependence of the AlGaN/SiO_2 interface potential close to V_{so}, we performed a CV simulation using a Poisson solver based on Ref. 16, see Fig. 3. V_{th} and V_{so} values were adjusted by varying the magnitude of the positive fixed charge at the AlGaN/dielectric interface[10] and the density of acceptor (i.e., negative when occupied by electron) traps at the interface. The trap distribution was chosen narrow and close to the conduction band edge of AlGaN in order, the V_{th} and V_{so} values in the simulated curves approach those from the experiments. We consider the trap occupancy follows the *ac* signal (i.e., low frequency limit). The corresponding band diagram for different biases (inset of Fig. 3) shows a potential pinning above V_{so}, see discussions below. As well, we would like to point out that in the regime $V \gg V_{th}$ (i.e., high density of 2DEG), there is negligible response of traps in the GaN buffer. These traps cannot change their occupancy due to buffer potential shielding by 2DEG.[9]

III. LUMPED ELEMENT MODELING

A. Qualitative analysis in the spill-over regime: No traps

Here, we consider a simplified small signal LEM of the gate stack in the spill-over regime, without considering the effect of traps. We consider a high conductivity of the 2DEG in GaN channel, acting as an ideal metal electrode. Similarly like in Ref. 14, the model consists of the dielectric capacitance, C_{ox}, connected in series with the parallel combination of the small-signal resistance, R_{br} (or conductance, $G_{br} = 1/R_{br}$), of the AlGaN barrier and the barrier capacitance, C_{br}, see Fig. 1(b). The equivalent parallel capacitance, C_p, and conductance, G_p, can be expressed as (see Fig. 1(c))

$$C_p = \frac{C_{ox}\left[1 + \omega^2 R_{br}^2 C_{br}(C_{ox} + C_{br})\right]}{1 + \omega^2 R_{br}^2 (C_{ox} + C_{br})^2}, \tag{1}$$

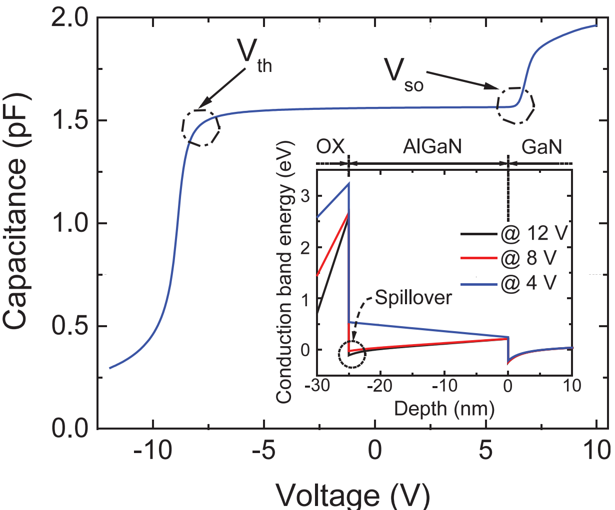

FIG. 3. CV curves simulated by a Poisson solver. Inset: Corresponding band diagram with the voltage below (4 V) and above V_{so} (8 and 12 V). Eight acceptor interface defect levels with the same density of 9×10^{10} cm^{-2}, equally distributed in energy in the interval E_c(AlGaN)-0.1 eV to E_c(AlGaN)-0.01 eV are considered to simulate a density of states.

$$G_p = \frac{\omega^2 C_{ox}^2 R_{br}}{1 + \omega^2 R_{br}^2 (C_{ox} + C_{br})^2}. \tag{2}$$

It can be seen from (1) that in the low frequency limit (i.e., angular frequency $\omega \to 0$) $C_p \to C_{ox}$, while for $\omega \to \infty$, C_p is a series combination of C_{ox} and C_{br} (i.e., $C_p = C_{ox}*C_{br}/(C_{ox} + C_{br})$). This frequency dependence occurs due to term containing R_{br} in (1) and can explain the drop of the capacitance with frequency above V_{so} in Fig. 2. Physically, the capacitance increase up to C_{ox} in the spill-over regime occurs due to the decrease of the barrier resistance R_{br} (we consider a bias dependent R_{br}) or "short-circuiting" of the AlGaN barrier. Indeed, looking at (1), when $R_{br} \to 0$ (i.e., high AlGaN barrier transparency for electrons), then, $C_p = C_{ox}$, while for $R_{br} \to \infty$ (i.e., low transparency) $C_p = C_{ox}*C_{br}/(C_{ox} + C_{br})$. Importantly, for the case of a finite value of R_{br}, a frequency dispersion described above occurs, even without considering the response of traps.

Furthermore, G_p as a function of R_{br} peaks at

$$R_{br,max} = \frac{1}{G_{br,max}} = \frac{1}{\omega(C_{ox} + C_{br})}, \tag{3}$$

which is the basis of origin of conductance peak for low frequency observed near V_{so} in Fig. 2. As the forward bias increases the barrier resistance, R_{br} decreases from a high value to a low value. At higher frequencies, R_{br} is not sufficiently low (see (3)), so a peak in G_p does not appear (see Fig. 2).

We call the frequency dispersion in (1) and (2), the *intrinsic response of the gate stack*. In Sec. III B, we extend the LEM to the whole bias region including 2DEG depletion.

B. CV and GV simulation in the whole bias regime: No traps

Here, we propose an extended, still trap-free, gate stack model covering the whole bias regime. Rigorously, the regions below but also outside the gate should be treated as distributed RC networks. For simplicity, we adapted the treatment of Ref. 17 for the situation of MOSFET in inversion to our case of accumulation type MIS structure. We replaced distributed substrate capacitance, channel resistances under the gate and outside-the-gate regions by a simple parallel combination of depletion capacitance C_d (i.e., due to 2DEG depletion below the gate) with serial connection of the above-mentioned C_s and an effective channel resistance R_c (Fig. 1(d)). Although this is a rough, first order approach,[17] it provides a qualitative estimation of the effect of 2DEG modulation to the total response for $V \ll V_{so}$. The possible substrate resistance[18] and transmission line effects[17] are neglected. This is justified as we limit our analysis to frequency $\leq$1 MHz, the substrate is highly doped and the measured limiting values of capacitances (i.e., C_{ox} and $C_{ox}*C_{br}/(C_{ox} + C_{br})$) are consistent with the calculated ones from the structure geometry and permittivity. Our LEM can also be applied for structures with lateral Ohmic electrode, in which C_s in Fig. 1(d) will be short-circuited.

Figs. 4(a) and 4(b) shows the simulated equivalent C_p and G_p for the model of Fig. 1(d), with bias dependent R_{br},

[This article is copyrighted as indicated in the article. Reuse of AIP content is subject to the terms at: http://scitation.aip.org/termsconditions. Downloaded to] IP: 128.131.87.29 On: Wed, 28 Jan 2015 15:02:39

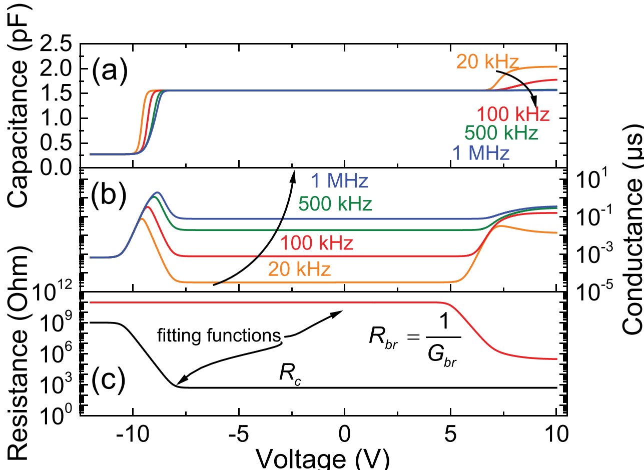

FIG. 4. Numerical simulations (in Matlab[T]) of the equivalent parallel capacitance C_p (a) and conductance G_p (b) as a function of voltage with the frequency as parameter, for the case without traps. The voltage dependences of R_{br} and R_c, used as approximate fitting functions, are shown in (c); $C_{ox} = 2.06$ pF, $C_{br} = 6.44$ pF, $C_s = 10$ nF.

R_c, and C_d. The bias dependence of R_{br} and R_c was simulated with sigmoidal-like functions from a maximum to minimum value, so that the experimental results in Fig. 2 are fitted approximately. Correspondingly, the regions where R_{br} and R_c vary with bias are around V_{th} and V_{so}, respectively, see Fig. 4(c). The lowest value of R_{br} (i.e., the asymptotic value at high forward bias) of 200 kΩ is chosen to be consistent with the dynamic resistance dV_g/dI_g of the Schottky diode, where I_g is the forward biased leakage current (≈120 nA at $V_g \approx 0.7$ V), which is related to the AlGaN barrier transparency above V_{so}. For a more detailed comparison, one would need to consider a bias voltage rescaling in the MIS and Schottky structures for the condition of the same band bending in the AlGaN barrier (i.e., the same transport via the barrier) and take the I_g value at this rescaled voltage value. The minimal value of R_c is consistent with the value of sheet resistance of the 2DEG of 500 Ω/□, which is a first order comparison, not considering possible corrections for geometrical factors. For the bias dependence of C_d, we used a procedure proposed in Ref. 17 but the simulation shows that the main features in C_p and G_p near V_{th} are mostly determined by the bias dependence of R_c and not of C_d. We would like to notice that for bias $V \gg V_{th}$ (so 2DEG accumulation and spill over regime), the frequency response of C_p and G_p are not affected by the LEM parts composed of C_d, R_c, and C_s for $R_c < 1000$ Ω and $C_s > 1$ nF.

The model can explain the following experimental features:

(1) The shift in V_{so} in $C_p(V)$ curve with the increased frequency, which is determined by the width of the transition region in R_{br} (compare Fig. 2 and Figs. 4(a) and 4(c)).
(2) The decrease in the capacitance plateau values at $V > V_{so}$, which is due to finite value of R_{br} for $V > V_{so}$.
(3) The small frequency dispersion in $C_p(V)$ curves near V_{th} and the finite capacitance value in depletion for $V < V_{th}$, the former behavior being mainly due to R_c-related effects.
(4) The peaks (both near V_{th} and V_{so}) and plateaus in $G_p(V)$ curves are also qualitatively reproduced but their absolute values are underestimated. Analogously as G_p peak near V_{so} is due to decrease of R_{br} with bias (see Sec. III A), the G_p peak near V_{th} is due to decrease of R_c with voltage rise. The plateau values in conductance in the range (≈−7 V)–(≈ 5 V) depend basically on the value of R_c and are not influenced by the LEM of the AlGaN barrier. The discrepancies between calculations and measurements in terms of absolute values are attributed to model simplifications.
(5) The frequency-induced shift of the onset voltage for the conductance rise is also qualitatively in agreement with experiments. The shape of the G_p-V curve for $V > V_{so}$ depends on the shape of the $R_{br}(V)$ function, but the more exact extraction of $R_{br}(V)$ is beyond the scope of this paper.

C. Lumped element model with traps

Here, we present a small-signal LEM of the gate stack, including the response of the interface states, valid for the spillover region. We do not consider the effect of channel resistance, similarly as in Sec. III A. Figs. 1(e) and 1(f) show the extension of model in Fig. 1(b) to the case of a single and multiple trap levels, respectively. A small signal model of a single defect level with a single trap time constant consists of serial combination of frequency independent trap capacitance, $C_{t,s}$, and conductance, $G_{t,s}$ (the usual parallel representation of the defect admittance uses frequency dependent elements)[19]

$$C_{t,s} = A\frac{q^2}{kT}f(1-f)D_{it}, \tag{4}$$

$$G_{t,s} = \frac{C_{t,s}}{\tau_t} \tag{5}$$

with D_{it} being the density of traps in cm^{-2}, A is the capacitor area, f is the Fermi-Dirac defect occupancy factor dependent basically on the defect energy position, τ_t is the defect time constant dependent on defect ionization energy and capture cross section and f,[19] q is the elementary charge, k is the Boltzman constant, and T is the temperature. In the case of multiple defect levels (Fig. 1(f)), τ_t, D_{it} and f-factor will be different for each serial branch in the LEM. In contrast to model of Ref. 14, where the defect-related elements are in series with the barrier capacitance and conductance, our model considers a parallel combination of the AlGaN barrier parameters with the defect branch. This is physically reasonable as for the limit of no interface states (i.e., $C_{t,s} = 0$, $G_{t,s} = 0$), there is still remaining the intrinsic frequency response due to the AlGaN barrier (see Sec. III A).

In order to take into account the finite, bias-dependent barrier conductance at the lateral spatial positions of the interface defect (i.e., in the interface plane), we consider a barrier dynamical conductance $G_{br,T}$ in series with the defect elements, see Fig. 1(e). For example, Lagger *et al.* suggested that the barrier could act as rate limiter for the trapping.[8] Consequently, the effective capture time constant can be

[This article is copyrighted as indicated in the article. Reuse of AIP content is subject to the terms at: http://scitation.aip.org/termsconditions. Downloaded to] IP: 128.131.87.29 On: Wed, 28 Jan 2015 15:02:39

given as $\tau_{t,eff} = \tau_t + \tau_{barrier}$.[8] Looking at defect branch in Fig. 1(e), it can be represented as

$$\tau_{t,eff} = C_{ts} * (1/G_{t,s} + 1/G_{br,T}), \tag{6}$$

where $\tau_{barrier} = C_{t,s}/G_{br,T}$ is the barrier contribution to the time constant.

Furthermore, for the case of multiple defects, Eqs. (4) and (5) show that as the bias is swept, defects with different energy positions will respond. In practice, we suppose that only traps from a very limited energy region will respond at forward bias. The bottom energy is limited to a moment, where $G_{br,T}$ is sufficiently high so that the trap can start to respond. The upper energy is limited by the pinning of the interface potential above V_{so}, see Fig. 3. Looking at the band diagram in Fig. 3 and making similarity to Si/SiO_2 systems,[20] it is possible that also localized states above the AlGaN conduction band minimum, but within the SiO_2 forbidden gap, can be involved in the response.

D. CV modeling with traps

Besides the V_{so} shift due to intrinsic response of the gate stack, the traps can indeed influence the V_{so} shift.[14] We took LEM of Fig. 1(f) considering a continuous distribution of traps and use (4) and (5) with $f = 0.5$.[19,21] For a proper modeling, we would need to know how the interface potential depends on the applied forward bias. For simplicity, we consider a continuous trap density distribution over the applied voltage range of 5–10 V. Due to bias dependence of $G_{br,T}$, the traps begin to respond only around V_{so} (see the discussion above), so such a treatment is justified. The τ_t value was chosen to be 1 ns so that the traps can respond to the *ac* signal. Fig. 5 compares the frequency dependent CV curves for four trap concentrations. Looking at the low frequency CV curve (20 Hz) at $D_{it} = 5 \times 10^{10}\,\text{cm}^{-2}$, a small hump starts to be visible in the C_p-V curves due to the trap response. This can be explained using the transformation of the defect-related branch in Fig. 1(e) to an equivalent parallel representation[19] with the capacitance $C_{t,p} = C_{t,s}/[1 + (\omega\tau_{eff})^2]$ (see Fig. 1(g)). At low frequencies, $C_{t,p} \approx C_{t,s}$ and taking (4), one obtains values of $C_{t,p} \approx 1.6\,\text{pF}$, which becomes comparable to $C_{br} = 6.44\,\text{pF}$; therefore, the trap response starts to be visible in the total response. At concentration, $D_{it} = 2 \times 10^{11}\,\text{cm}^{-2}$, $C_{t,p} \approx C_{br}$, and the hump due to traps increases. For $D_{it} = 1 \times 10^{12}\,\text{cm}^{-2}$ and higher the CV curve does not change anymore with D_{it}, since $C_{t,p} \gg C_{br}$ and the trap response therefore dominates (notice $C_{br} + C_{t,p}$ is in series with C_{ox}). Importantly, the frequency shift of V_{so} toward higher bias can be observed also for the case with traps. Although inclusion of traps in the LEM can provide us another degree of freedom in fitting the experiment of Fig. 2 better, such an analysis is beyond the paper scope.

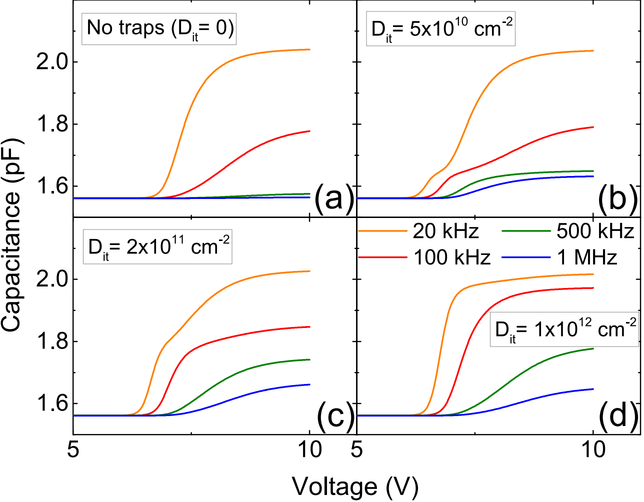

FIG. 5. Simulated C_p-V curves with frequency as parameter for four indicated trap densities. The data of (a) for $D_{it} = 0$ are the same as in Fig. 4(a). Values used in simulation: $\tau_t = 1\,\text{ns}$ is the same for all traps, $f = 0.5$, $G_{br,T}(V) = 4 \times G_{br}(V)$, otherwise as in Fig. 4.

The above analysis indicates that there is complex interplay between the intrinsic response of the gate stack and the response of traps. Both effects take place simultaneously and results in comparable effects for the trap density of the order of $10^{11}\,\text{cm}^{-2}$. Our results could also explain why the second capacitance onset is sometimes observed in the literature and sometimes not. As the barrier dynamic resistance, R_{br} is strongly material and design dependent, the small-signal response can differ from structure to structure. Different transport processes through the AlGaN barrier like thermoionic emission, defect-assisted tunneling, conduction via extended defects,… can prevail in different structures.[8,22–26] Even if free electrons are accumulated at the III-N barrier/dielectric interface, if the frequency and barrier resistance are sufficiently high, the free electrons will not follow the *ac* signal, meaning that there will be no electron exchange between the 2DEG in GaN and the accumulated electrons at the AlGaN/dielectric interface. As a result of such a non-equilibrium situation, one would measure series combination of C_{ox} and C_{br} instead of C_{ox}. For example, in the simple CV and band diagram simulation based on Poisson solver given in Fig. 3, an equilibrium condition is always established for free carriers (i.e., constant Fermi-level assumption; electron concentration in AlGaN follows the *ac* bias), as no constrain is considered implicitly for the barrier conductivity. The effect of finite barrier conductivity can only be incorporated by considering additional kinetic equations.

E. Conductance modeling with traps

Taking into account, the LEM without traps from Fig. 1(b), one can find that a peak occurs in the G_p/ω dependence as a function of ω at

$$\omega_{max} = \frac{1}{R_{br}(C_{ox} + C_{br})} = \frac{G_{br}}{(C_{ox} + C_{br})} \tag{7}$$

with G_p/ω reaching the peak value

$$(G_p/\omega)_{max} = \frac{1}{2}\frac{C_{ox}^2}{(C_{ox} + C_{br})}. \tag{8}$$

This maximum value in (8) is independent of R_{br} (or $1/G_{br}$) and is of the order of C_{ox}, which is crucial for further discussion of the effect of traps.

[This article is copyrighted as indicated in the article. Reuse of AIP content is subject to the terms at: http://scitation.aip.org/termsconditions. Downloaded to] IP: 128.131.87.29 On: Wed, 28 Jan 2015 15:02:39

In the following, the G_p/ω vs. ω for the LEM with one type of trap level (i.e., model of Fig. 1(e)) is analyzed numerically since the full analytical solution is cumbersome. For the simplicity, we consider the trap energy is located at the Fermi level, i.e., $f = 0.5$ in (4). Like in Sec. III D, the τ_t value is chosen to be 1 ns so that the trap responds to the *ac* signal. Fig. 6(a) shows 2D "amplitude" plot of G_p/ω as a function of ω and D_{it}. Cross-sections of G_p/ω vs. ω with D_{it} as parameter are given in Fig. 6(b). For $D_{it} < 1 \times 10^9$ cm^{-2}, one observes one peak at $\omega_{max,1} = G_{br}/(C_{br} + C_{ox})$, see (7). At high D_{it} (practically for $D_{it} > 10^{12}$ cm^{-2}), there is again one peak at $\omega_{max,2} = (G_{br} + G_{br,T})/(C_{br} + C_{ox})$. This can be easily understood as for $D_{it} \to \infty$, $C_{t,s}$, and $G_{t,s}$ go to infinity too. The elements in the defect branch in the schematics of Fig. 1(e) will thus reduce to $G_{br,T}$, meaning that the branch will have pure conductive nature (i.e., no imaginary component). In this case, the conductances G_{br} and $G_{br,T}$ in Fig. 1(e) will sum and one can use the same Eqs. (7) and (8) to express ω_{max} and $(G_p/\omega)_{max}$, respectively. In both cases of $D_{it} \to 0$ and $D_{it} \to \infty$, the maximum value of the G_p/ω peak reaches the value determined by (8), see Fig. 6(b). In the intermediate case, i.e., for finite D_{it}, two peaks or a peak with a shoulder can encounter in G_p/ω vs. ω dependence, with the G_p/ω peak value lower than (8). Our simulations also show that changing τ_t or $G_{br,T}$ does not change qualitatively the above features.

The analysis above shows that the direct use of G_p/ω value for determination of defect density at the AlGaN/dielectric interface is not suited for MIS-HEMTs. We emphasize that $(G_p/\omega)_{max}$ does not scale linearly with D_{it} (see Fig. 6(b)) and that the saturation occurs at the limiting value of (8), which leads to underestimation of the defect densities, in accordance to Ref. 14. Even in the case of $D_{it} = 0$, one obtains a conductance peak due to the intrinsic barrier response. So for the proper evaluation of the interface state density in MIS-HEMTs from the conductance measurement, it would be necessary to make a complex de-embedding of the trap response from the barrier response. Such a de-embedding procedure does exist for the case of pure MOSFETs,[19,27] where the channel electrons are in contact with the interface states but not yet for the MIS-HEMTs.

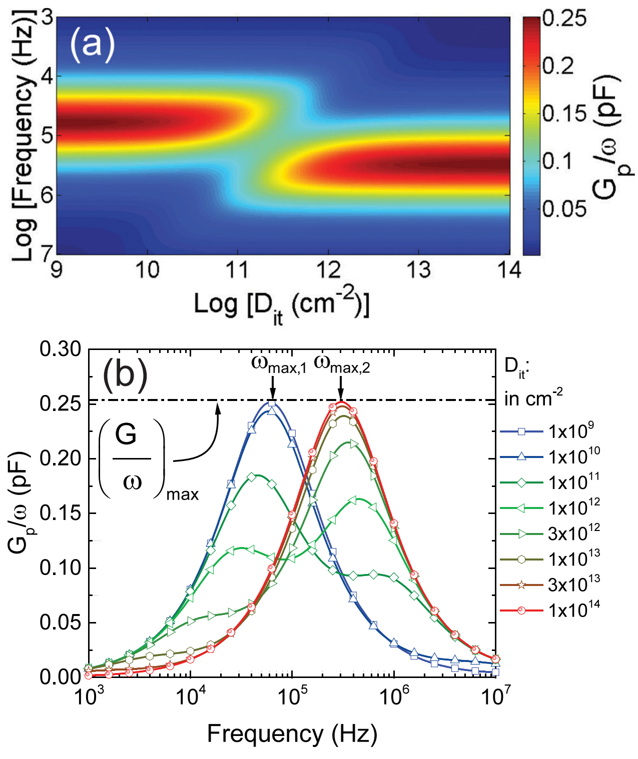

FIG. 6. (a) Two-dimensional plot of G_p/ω as a function of D_{it} and frequency showing two main peaks in the distribution. (b) Dependence of G_p/ω vs. frequency with defect density D_{it} as parameter. The maximum value $(G_p/\omega)_{max}$ is indicated. Values used for simulation: $R_{br} = 1/G_{br} = 200$ kΩ, $G_{br,T} = 20$ μS, $\tau_t = 1$ ns, $f = 0.5$, otherwise as in Fig. 4.

IV. CONCLUSIONS

We have performed a theoretical analysis and first order evaluation of admittance in the case of MIS-HEMT gate stack taking into account both the voltage-dependent barrier resistance and trap effects. Using a LEM, we have found a complex interdependence between the intrinsic response of the gate stack and the contribution of traps, which can lead to comparable effects, both in capacitance and conductance. In particular, the frequency-induced shift in the second onset in CV curve in the spill-over regime can be alternatively explained by the intrinsic frequency response of the gate stack using a bias-dependent AlGaN barrier resistance R_{br}, without considering the effect of traps. This has to be taken into account in the trap extraction from the shift in V_{so}. The trap density extraction from the shift in V_{th} or using stress-recovery experiments[8] is however appropriate. Furthermore, the conductance also depends in a complex way on barrier resistance and trap density and the maximum value of G_p/ω is limited to the order of C_{ox}, independent of defect density. Therefore, without the correction to C_{ox}, C_{br}, and R_{br}, the direct use of G_p/ω peak value for trap density evaluation can lead to underestimation of D_{it} values, which is in accordance with Ref. 14. Moreover, the conductance peak appears even without traps, just due to the intrinsic gate stack response. Because of this complexity and the above saturation of $(G_p/\omega)_{max}$ value, we think that the conductance method is of little use for trap density evaluation in MIS-HEMTs unless special de-embedding methods are developed. The conductance method can however be used for trap evaluation in true GaN MISFETs (or MOSFETs), where the electron channel is in direct contact to interface traps.[18,24,27] We believe that our work is a basis for future works clarifying the complex interplay between the small-signal response of the AlGaN barrier and the traps in MIS-HEMTs, where more complex models of the gate stack with traps can be employed. Using such models, the voltage dependence of R_{br} could be extracted from experiments using complex fitting procedures. This might give the opportunity to compare transport properties of different III-N barriers leading to MIS-HEMT optimization. Without assuring that it is principally possible, we also want to point out that the stability of the threshold voltage can be achieved by (i) decreasing the density of interface states or shifting their response either to very short (immediate response, fast capture and emission) or very large (no response, no carrier capture) time scale and/or (ii)

[This article is copyrighted as indicated in the article. Reuse of AIP content is subject to the terms at: http://scitation.aip.org/termsconditions. Downloaded to] IP: 128.131.87.29 On: Wed, 28 Jan 2015 15:02:39

simultaneous increase in V_{so} above the maximum applied gate voltage and having negligible barrier conductivity below V_{so}, i.e., no available electrons for capturing at the AlGaN/dielectric interface.

[1]M. A. Khan, X. Hu, G. Sumin, A. Lunev, J. Yang, R. Gaska, and M. S. Shur, IEEE Electron Device Lett. **21**, 63 (2000).
[2]S. Yang, Z. Tang, K.-Y. Wong, Y.-S. Lin, C. Liu, Y. Lu, S. Huang, and K. J. Chen, IEEE Electron Device Lett. **34**, 1497 (2013).
[3]Y. Hori, Z. Yatabe, and T. Hashizume, J. Appl. Phys. **114**, 244503 (2013).
[4]M. Miczek, C. Mizue, T. Hashizume, and A. Adamowicz, J. Appl. Phys. **103**, 104510 (2008).
[5]P. Gangwani, S. Pandely, S. Haldar, M. Gupta, and R. S. Gupta, Solid-State Electron. **51**, 130 (2007).
[6]S. Heikman, S. Keller, D. S. Green, S. P. DenBaars, and U. K. Mishra, J. Appl. Phys. **94**, 5321 (2003).
[7]S. Huang, S. Yang, J. Robers, and K. J. Chen, Jpn. J. Appl. Phys. **50**, 110202 (2011).
[8]P. Lagger, M. Reiner, D. Pogany, and C. Ostermaier, IEEE Trans. Electron Devices **61**, 1022 (2014).
[9]P. Lagger, A. Schiffmann, G. Pobegen, D. Pogany, and C. Ostermaier, IEEE Electron Device Lett. **34**, 1112 (2013).
[10]S. Ganguly, J. Verma, G. Li, T. Zimmermann, H. Xing, and D. Jena, Appl. Phys. Lett. **99**, 193504 (2011).
[11]M. Esposto, S. Krishnamoorthy, D. N. Nath, S. Bajaj, T. H. Huang, and S. Rajan, Appl. Phys. Lett. **99**, 133503 (2011).
[12]M. Tapajna and J. Kuzmik, Appl. Phys. Lett. **100**, 113509 (2012).
[13]M. Capriotti, A. Alexewicz, C. Fleury, M. Gavagnin, O. Bethge, D. Visalli, J. Derluyn, H. D. Wanzenbök, E. Bertagnolli, D. Pogany, and G. Strasser, Appl. Phys. Lett. **104**, 113502 (2014).
[14]S. Yang, Z. Tang, K. Y. Wong, Y. S. Lin, Y. Lu, S. Huang, and K. J. Chen, Int. Electron Dev. Meet. Tech. Dig. **2013**, 13–152.
[15]P. Lagger, P. Steinchifter, M. Reiner, M. Stadtmüller, G. Denifl, A. Naumann, J. Müller, L. Wilde, J. Sundqvist, D. Pogany, and C. Ostermaier, Appl. Phys. Lett. **105**, 033512 (2014).
[16]J. E. A. Whiteaway, IEE Proc. **130**, 165 (1983).
[17]E. H. Nicollian and A. Goetzberger, IEEE Trans. Electron Devices **12**, 108 (1965).
[18]X. Liu, H.-C. Chin, L.-S. Tan, and Y.-C. Yeo, IEEE Trans. Electron Devices **58**, 95 (2011).
[19]E. H. Nicollian and J. R. Brews, *MOS (Metal Oxide Semiconductor) Physics and Technology* (Wiley Classics Library, 2002).
[20]Z. Ji, J. F. Zhang, W. D. Zhang, B. Kaczer, S. D. Gendt, and G. Groeseneken, IEEE Trans. Electron Devices **59**, 783 (2012).
[21]F. Ducroquet, O. Engström, H. D. B. Gottlob, J. M. J. Lopes, and J. Schubert, ECS Trans. **45**, 103 (2012).
[22]S. M. Sze and K. K. Ng, *Physics of Semiconductor Devices* (Wiley and Sons, 2007).
[23]H. Zhang, E. J. Miller, and E. T. Yu, J. Appl. Phys. **99**, 023703 (2006).
[24]E. J. Miller, E. T. Yu, P. Waltereit, and J. S. Speck, Appl. Phys. Lett. **84**, 535 (2004).
[25]D. Yan, H. Lu, D. Cao, D. Chen, R. Zhang, and Y. Zheng, Appl. Phys. Lett. **97**, 153503 (2004).
[26]A. Fontserè, A. Pérez-Tomés, M. Placidi, J. Liobet, N. Baron, S. Chenot, Y. Cordier, J. C. Moreno, V. Iglesias, M. Porti, A. Bayerl, M. Lanza, and M. Nafrìa, Appl. Phys. Lett. **101**, 093505 (2012).
[27]R. Engel-Herbert, Y. Hwang, and S. Stemmer, J. Appl. Phys. **108**, 124101 (2010).

[This article is copyrighted as indicated in the article. Reuse of AIP content is subject to the terms at: http://scitation.aip.org/termsconditions. Downloaded to] IP: 128.131.87.29 On: Wed, 28 Jan 2015 15:02:39